STRUCTURE, PHASE TRANSFORMATIONS, AND DIFFUSION

Effect of Phase Formation on Mechanical Properties of the Joint AA6061 to AA2024 by TLP

A. Anbarzadeh[a]**, H. Sabet**[b, *]**, and A. R. Geranmayeh**[a]

[a] *Department of Materials Engineering, South Tehran Branch, Islamic Azad University, Tehran, 1584715414 Iran*
[b] *Department of Materials Engineering, Karaj Branch, Islamic Azad University, Karaj, 3149968111 Iran*
*e-mail: h-sabet@kiau.ac.ir

Abstract—In this research, diffusion bonding was employed to joint AA2024 and AA6061 alloys. To select the alloy material of the interlayer, the atomic diffusion of tin, zinc, and gallium elements was modeled at a concentration of 90.1 wt % in pure aluminum. According to the modeling results, tin was selected as the main element of the interlayer alloy. Diffusion bonding was carried out in a tube furnace at a heating rate of 5°C/min under vacuum (7.5×10^{-3} Torr) and the temperature of 453°C for 210 min for Sn−5.3Ag−4.6Bi interlayer. This experiment was performed considering one interlayer with different thicknesses (20, 50, and 70 μm). Joints were assessed by SEM, and elemental mapping. Ag_3Al, $Mg_{45}Al_{40}Ag_{15}$ inter-metallic compounds, Sn-rich in solid solutions, and Sn + Cu_6Sn_5 phase were formed at the joint site of the interlayer. The maximum tensile strength of the samples with a joint thickness of 20 μm was 52 MPa after 210 min. By the increase of the Sn−5.3Ag−4.6Bi interlayer thickness (20−70 μm), the average unit tensile stress showed a decline. The effect of the interlayer thickness (20, 50, 70 μm) was investigated on the hardness, strength, and particle size as well as the joint phases.

INTRODUCTION AND RESERCH METHODS

AA2024 is known as a corrosion-resistant alloy with a Cu content of 4 wt %. With a density of 2.7 g/cc, it has exhibited precipitation hardening potentials [1]. Its tensile yield strength was also measured as 75.8 MPa [2]. Solidus temperature of AA2024-O is 502°C [1]. In this investigation is used Transient Liquid Phase (TLP) process, because AA2024 alloy has weak weldability. The 4 stages of the Transient Liquid Phase (TLP) process: 1—Heating, 2—Melting of the interlayer, 3—Isothermal solidification, and 4—Homogenization [3]. For the process to be TLP, it is not necessary for the homogenization stage to be completed. Other letters of the TLP process, depending on the stage or liquidous temperature of the filler metal, include TLP welding, TLP Brazing, TLP soldering, Diffusion Brazing and Diffusion Soldering [4−6]. The optimal temperature for the TLP process is between the complete annealing temperature and solidus temperature of AA2024 alloy that mean value is 457°C [1, 2]. Beyond this temperature, the solubility of copper deposits will be enhanced which may affect the heat treatment capability of the alloy. Noteworthy, the eutectic temperature of Al−Mg and Al−Cu are 450 and 548°C, respectively. Exceeding the eutectic temperature of Al−Mg will cause a higher Mg solubility which can help in the formation of ɣ deposits in the interlayer after the junction formation process [7]. Alloy AA2024 is prone to hot cracking. TLP bonding has been employed for joining the alloys with high susceptibility to hot cracking [8]. Moreover, the tensile yield strength and solidus temperature of AA6061-O are 55.2 MPa and 582°C, respectively [9]. In this regard, designing an appropriate interlayer alloy with no deleterious phases and a smaller melting point (compared to the base metal) is of crucial significance [10]. The evolution process of TLP bonding of precipitation hardening aluminium alloys involve Joining Al7075 to Ti−6Al−4V by a copper interlayer with a thickness of 22 μm using TLP method, which led to a bond strength of 19.5 MPa after 30 min. Alhazaa et al. [11] and Alhazaa and Khan [12] used Sn−3.6Ag−1Cu interlayer. Sn−10Zn−3.5Bi and Sn−4Ag−3.5Bi films (thickness of 50 μm) were employed as interlayer for TLP joining of Al7075 to Ti−6Al−4V which resulted in the respective bond strength of 30 and 36 MPa [13, 14]. Diffusion bonding of Al2024 to Ti−6Al4V was also achieved by Cu/Sn/Cu interlayer with a bond strength of 37 MPa at 510°C under vacuum (7.5×10^{-5} Torr) for 60 min bonding time [15]. TLP bonding of dissimilar alloys (Al2024 and Ti−6Al−4V) was successfully carried out using Cu−22Zn interlayer

at 510°C under the vacuum (5.6×10^{-7} Torr) for 60 min bonding time which resulted in the maximum tensile strength of 37 MPa [16]. Successive TLP bonding of Al2024 to Ti−6Al−4V was also reported utilizing Sn−5.3Ag−4.2Bi interlayers (thickness of 50 μm) which led to the bond strength of 62 MPa in the second stage at 453°C [17]. Heat distribution was modeled in the TLP joining of AA2024-T4 to AA6061-T6. The heat distribution in the base metal at 253°C was simulated one- and two-dimensionally. Sn−2.5Bi interlayer with two thicknesses (50 and 70 μm) was experimentally evaluated at 253°C in terms of microstructure and cross-section, considering the EDS (Cu) element line [18]. A one-dimensional mathematical model (method of separation of variables) was also proposed for predicting the redistribution of the solute within the TLP bonding process of Al−Cu alloy [10]. Also, the relationship between temperatures of melting and crystallization for crystal-liquid phase transition has been investigated by Mangomedov [19]. AA2024-T4 and AA6061-T6 alloys were soldered by diffusion bonding, using Sn−2.4Bi foil (50 μm) as the interlayer. The tensile strength of the soldering was 12.3 MPa for Sn−2.4Bi interlayer (50 μm) after 210 min (at 253°C) [20]. By increasing the bonding time, the Cu_6Sn_5 compound was formed in the sandwich Cu/Sn/Cu system under the TLP process [21]. Cu/Sn/Cu TLP system was investigated which showed the formation of Cu_6Sn_5 compound at the joint by prolonging the process [21, 22]. The reason for adding Ag to the interlayer alloy was that it prevented the accumulation of Cu at the Al grain boundaries and the formation of the brittle and continuous Al_2Cu phase along the aluminum grain boundaries. It also strengthens the joint by forming reinforcing silver sediments [23]. The proper concentration of Cu in the interlayer can result in the formation of the eutectic compound of Sn−Cu_6Sn_5 [24, 25]. White β-tin possesses a stable tetragonal crystal structure with a density of 7.31 g/cm³. By cooling down below 13.2°C, gray α-tin is formed with a cubic structure and a density of 5.77 g/cm³ with semiconducting features [26] also known as the tin pests [26, 27]. Cu, Fe, and Ni incorporation do not significantly affect the growth of tin pest. Reports on Cu are contradictory with more recent works suggesting the promoting role of Cu in tin pest [28, 29]. Little amounts of Bi (0.0035 wt %) can effectively inhibit the growth of tin pest [29]. Sn−0.3Bi, Sn−2.8Ag−10.1In, and Sn2.8Ag−20.3In are among the other promising candidates for soldering alloys [29]. The structure and phase composition of Al alloys have been studied by calculations and experimental methods [30−32]. This paper is devoted to a theoretical and experimental study of the diffusion alloying of AA2024 and AA6061 alloys using an interlayer, as the material of which, according to the results of a computer modeling selected tin. The experimental tests were conducted on

Sn−5.3Ag−4.6Bi foil with interlayer thicknesses of 20, 50, and 70 μm.

THEORETICAL ANALYSIS AND MATHEMATICAL FORMULATION

The thermal properties and mass diffusivities were assumed constant. This model is based on Fick's second law and the method of separating variables. The interlayer and Al base metal were initially at uniform solute concentration.

$$\partial C/\partial t = D\left(\partial^2 C/\partial x^2\right). \quad (1)$$

The boundary conditions:

$$C = C_i = 90.1 \text{ wt \%} \quad \text{at } t = 0; \quad (2)$$

$$\partial C/\partial t = 0 \text{ at } (x = 0 \text{ and } C = C_a = 45 \text{ wt \%}) \text{ at } x = L/2. \quad (3)$$

C_i: Concentration of Sn, Zn, or Ga in the interlayer at time zero. C_a: Concentration of Sn, Zn, and Ga at the interlayer boundary position at $t = 0$.
t: Time, D: effective solute diffusivity, C: Solute concentration. L: Characteristic length ($L = 0.1$ mm), x: Characteristic length. Using the following variable change:

$$W = C - C_a. \quad (4)$$

The boundary conditions and the governing equation are as follows:

$$\partial w/\partial x = D(\partial^2 w/\partial x^2); \quad (5)$$

$$W = C_i - C_a = W_i \quad \text{at } t = 0; \quad (6)$$

$$\partial w/\partial x = 0 \text{ at } (x = 0 \text{ and } W = 0) \text{ at } x = L/2. \quad (7)$$

Using the method of separation of variables $W(x, t) = f(x)g(t)$:

$$\frac{1}{Dg}\frac{dg}{dt} = \frac{1}{f}\frac{d^2 f}{dx^2} = -\lambda^2. \quad (8)$$

According to the symmetry:

$$\left.\frac{df}{dx}\right|_{x=0} = 0. \quad (9)$$

After performing a series of calculations, we will have:

$$W(x,t) = C(x,t) - C_a$$
$$= \sum_{n=0}^{\infty} \frac{4W_i}{(2n+1)\pi}(-1)^n \cos\frac{(2n+1)\pi x}{L} e^{-D\lambda_n^2 t} \quad (10)$$

$$\text{and } \lambda_n = ((2n+1)\pi)/L. \quad (11)$$

After drawing the diagram by the software (MATLAB & SIMULINK R2016b), the longitudinal origin should be transferred to the turning point (interlayer boundary position ($x = L/2$) at $t = 0$ s). Atomic diffusion modeling in pure Al is performed to

select the appropriate interlayer material. The properties required for modeling at 453°C are listed in Table 1.

EXPERIMENTAL

A temperature of 453°C (near the eutectic temperature of Al−Mg) was selected as the optimal temperature for modeling and experiments. Before selecting the interlayer material, the atomic diffusion of Ga, Zn, and Sn was modeled as the interlayer with the weight percentage of 90.1 wt % considering Al as the base metal. The boundary of the interlayer and the base metal with the solute content of 45 wt % was considered as the origin of the coordinate system. The modeling was carried out at four times of 1, 60, and 210 min as well as one day (for Sn). According to the modeling results, tin was selected as the main element in the interlayer alloy. After selecting the base elements in the interlayer, the other elements were selected based on the condition of the selected elements. Adding Bi to the interlayer improved wettability and prevented Tin pest at low temperatures [13, 29]. The reason for choosing silver alloy is to improve the bond strength by creating a deposition phase and preventing the formation of a brittle Al_2Cu phase at the aluminum grain boundaries [23]. Sn−5.3Ag−4.6Bi foil with thicknesses of 20, 50, and 70 μm was used as the interlayer. The interlayer foils are made of casted and rolled alloys. The reason for choosing this thickness of interlayer originates from the simulation results at 453°C for 210 min which predicts the thicknesses equal and below 23 μm as welding and higher than that as soldering. The model results should be validated by experiments. The tensile strength of the Sn−5.3Ag−4.6Bi interlayer was 66.3 MPa. Table 2 presents the chemical composition of the base metals. The wire cutting method was employed to cut the samples into 130 × 32 × 3 mm³ pieces for the strength test, and 16 × 25 × 3 mm³ pieces for SEM, hardness, and elemental mapping. The bonding surface alloys were made using 80 grit SiC finishing. The alloys and interlayers were ultrasonically cleaned (10 min, 35 kHz, and 0.5 A) using acetone. The heat treatment process was applied by a high-temperature horizontal carbonate tube furnace. Diffusion bonding was carried out at 453°C in an atmosphere control tube furnace at a heating rate of 5°C/min under vacuum (7.5 × 10⁻¹³ Torr) for different thicknesses (20, 50, and 70 μm) using Sn−5.3Ag−4.6Bi interlayer for 210 min. The samples are slowly cooled to room temperature in a vacuum furnace. The etching process was conducted for 12 s using an etchant solution encompassing 1.5 mL HCl, 2.5 mL HNO_3, 1 mL HF, and 95 mL distilled water. The effect of interlayer thickness of AA2024/AA6061 alloys was explored using scanning electron (AIS2300C) microscopic methods. Depending on the imaging site, voltage of 15 kV was employed to determine the elemental distribution and linear elemental map of the samples. Tensile strength was explored in two cases and the

Table 1. Diffusion of (Sn, Ga, Zn) at 453°C in Al [32, 33]

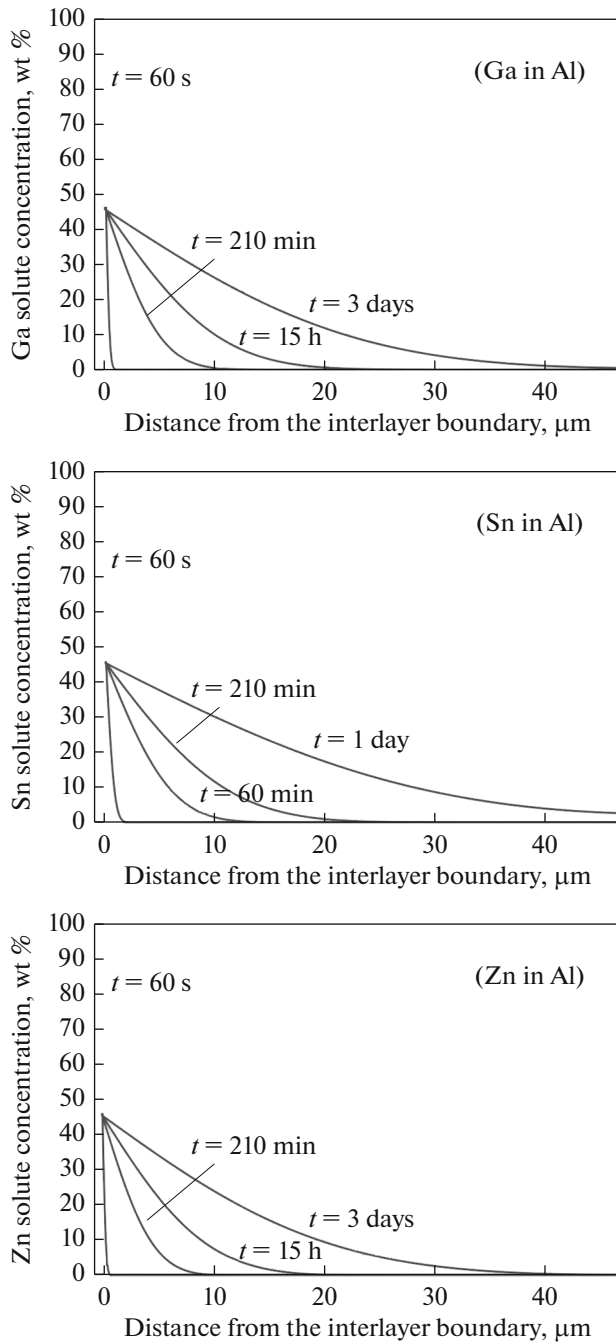| Element	D, m² s⁻¹
Sn	2.9×10^{-13}
Ga	0.6×10^{-13}
Zn	0.5×10^{-13}

Table 2. Chemical composition of the applied metals

Alloys	Elements, wt %						
	Al	Cu	Mg	Mn	Cr	Fe	Si
AA2024	Bal.	4.1	1.4	0.5	0.02	0.31	0.29
AA6061	Bal.	0.23	0.92	0.05	0.23	0.26	0.62

impact of interlayer thickness on the strength was assessed considering 5 samples. The changes in the tensile strength of the samples by bonding time were also investigated considering 4 specimens. Micro-Vickers hardness test was also employed to compare the modeled results for interlayer thicknesses of 20, 50, and 70 μm which is the most important validation test as the diffusion of Sn into Al base metal can decrement the hardness of the region. Micro Vickers hardness test was used for the produced samples. For this purpose, "Innova test NOVA 240 hardness tester" according to the reference standard of ASTM E384 (2017) test method was used. The application time for all checked points was 12 s. Applying excessive force to the joint, which contains a significant amount (90% by weight) of Sn, is cause a stiffness measurement error. Therefore, two different forces have been used to measure the hardness of the base metals and the location of the interlayer. The force applied to the peak loads of aluminum base metals is 2.942 N. And for the points of peak loads on the interlayer boundary and the interlayer of tin is 0.09807 N. The base metal was AA2024-T4 and AA6061-T6 before the bonding process.
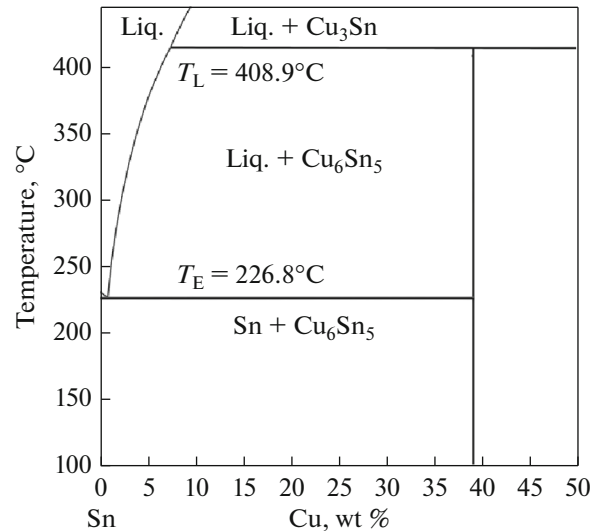
RESULTS AND DISCUSSION

The solute concentration distribution (Sn, Zn, or Ga) at 453°C is depicted in Fig. 1. Based on the modeling, Sn exhibited longer diffusion depth in the studied samples, thus it was considered as the base element in the interlayer. This model, however, fails in the cases where the interlayer thickness is below 23 μm as the process will be no longer soft soldering of transient liquid phase but rather changes into TLP welding which can enhance the strength and hardness of the joint. The reason could be the modeling results for Sn in Fig. 1 which estimated the atomic diffusion depth of 23 μm for Sn in pure aluminum at 453°C for 210 min. Sn−5.3Ag−4.6Bi alloy is a eutectic alloy.

The equilibrium phases diagrams Sn−Cu is shown in Fig. 2. The elemental mappings of the joint is shown

Fig. 1. Ga, Zn and Sn distribution at 453°C for different holding times.

Fig. 2. Sn−Cu Equilibrium phases diagrams [18].

Sn-rich in solid solutions, $AlAg_3$, and $Mg_{45}Al_{40}Ag_{15}$ inter-metallic compounds, and $Sn + Cu_6Sn_5$ phase in AA2024 and AA6061 alloy weld side. $Mg_{45}Al_{40}Ag_{15}$ was in the form of the Ag-rich $\gamma(Al_{12}Mg_{17})$ phase. As the thickness of the interlayer decreased, the size of the reinforcing particles significantly declined while their number showed an increment.

However, the XRD pattern did not confirm more specific phases such as Al_3Cu_2 and Ag_3Sn, but they may exist. By declining the thickness of the interlayer, the diameter of the reinforcing particles got smaller in the interlayer (from 11 μm in the samples with an interlayer thickness of 70 to 2 μm in the samples with an interlayer thickness of 20 μm) after 210 min of bonding time as depicted in Fig. 3. The number of particles however increased in the interlayer with better distribution (Fig. 5). Figure 5 shows the percentage of particles in the interlayer as a function of the interlayer thickness at 453°C and bonding time of 210 min. The mentioned thicknesses are the thickness of the interlayer after 210 min of the transient liquid phase at 453°C. The interlayer thickness decreased from 20, 50, and 70 μm before the process to about 2, 26, and 35 μm after TLP, respectively. The tensile strength of the bonding sample for an interlayer thickness of 70 μm was 4.1 MPa after 210 min. The maximum tensile strength of the sample with 50 μm thickness joint after 210 min was 7.3 MPa, another test shows this value as 6.2 MPa. The maximum tensile strength of the sample with 20 μm thick joint after 210 min was 52 MPa while another test showed it as 49 MPa. On the other hand, at a constant interlayer thickness, the strength increased with prolonging the process as tested for the interlayer thickness of 20 μm at bonding times of 150, 180, and 210 min. The tensile strength of the joints is shown in Fig. 6. The breaking point is also
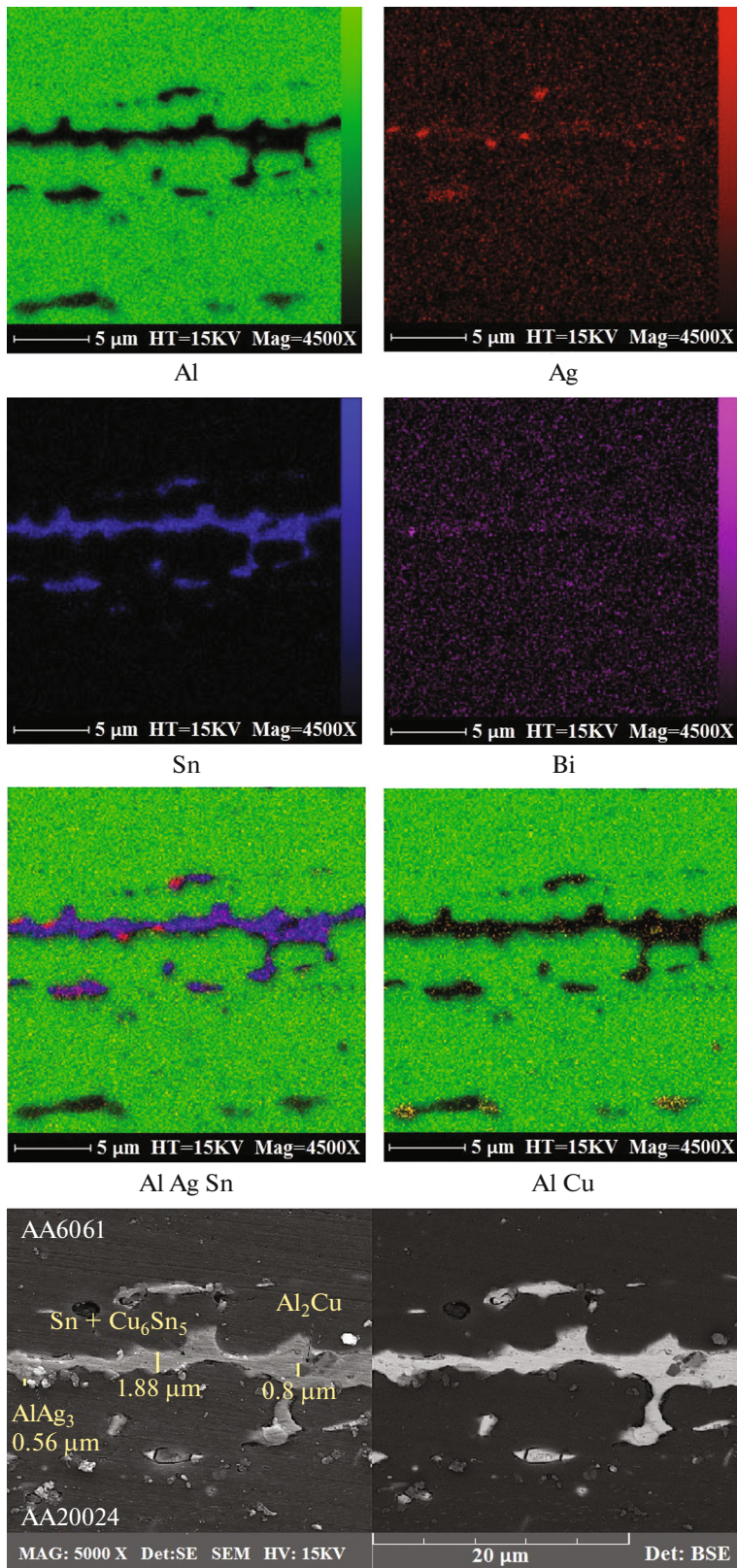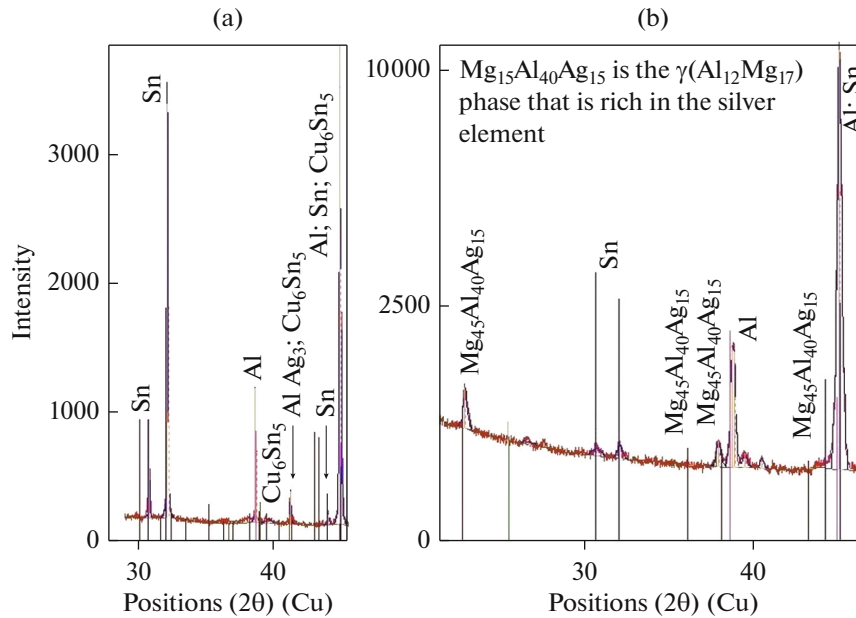
in Fig. 3 for the Sn−5.3Ag−4.6Bi interlayer. Bi was homogeneously distributed in base metals and the interlayer. Cu penetrated the interlayer more than Al. After performing the tensile test for the sample with 20 μm interlayer, the sample broke at the interface. X-ray diffraction pattern was taken from the fracture site of this sample. The x-ray diffraction patterns of both fracture surfaces are presented in Figs. 4a and 4b. X-ray diffraction patterns confirms the presence of

**Fig. 3.** Elemental mapping of the welding (thickness of 20 μm and bonding time of 210 min).

Fig. 4. X-ray diffraction patterns for Sn−5.3Ag−4.6Bi interlayer thickness of 20 μm, (a) Joint side of AA2024, and (b) Joint side of AA6061.

the interlayer and the base metals have higher strength than the interlayer. Hardness profiles of diffusion zone at bonding time of 210 min are shown in Fig. 7.

The results of the hardness test were used for model validation. The difference between the computational model and Sn−5.3−4.6Bi was considered as the computational error. Hardness at the joint was lower than in the base metals. For interlayers with thicknesses of 50 and 70 μm, the boundary stiffness on the AA6061, (or at the distance of 15 μm from the interlayer centre)

Fig. 5. Percentage of reinforcing particle area (Al Ag$_3$, Cu6Sn5, γ(Al$_{12}$Mg$_{17}$) and Al$_2$Cu) in the interlayer after TLP process.

was about 14−15.7 HV, whose atomic diffusion properties are closer to the pure aluminum. About 20 μm ahead of this interlayer boundary, i.e. at a distance of 35 μm from the interlayer centre, the hardness has increased and reached 27.3−29.1 HV. This is where, at the very beginning of the process, there was the interlayer boundary for the 70-μm-thick interlayer alloy.

According to the hardness results are shown in Figs. 4 and 5, the interlayer has moved about 15 ± 5 μm towards the centre of the interlayers. This is consistent with the modeling result which showed a penetration depth of 23 μm under similar conditions for the interlayer containing 90.1wt % Sn. But this modeling is not responsive for the interlayer thickness below 23 μm, such as the 20 μm interlayer tested. In such cases, there is no longer a transient liquid phase soldering process, but rather a transient liquid phase welding which increased the strength and hardness. Concerning the model, the Sn concentration of the interlayer was considered constant, supported by an endless source of tin. But as the boundary moved, the thickness of the interlayer narrowed and sufficient resources depleted to maintain a stable Sn penetration, thus, the two boundaries almost came together. Since AA2024 has more alloying elements than AA6061, the atomic penetration rate of tin in AA2024 was slower. This justifies the steeper slope of the hardness changes on the AA2024 alloy than the AA6061 alloy for the interlayer thicknesses of 50 and 70 μm. The presence of more alloying elements in AA2024 than AA6061 and pure aluminum reduced the penetration of tin in AA2024 (D: m^2/s: effective solute diffusivity). The error value of the model created for the atomic penetration depth
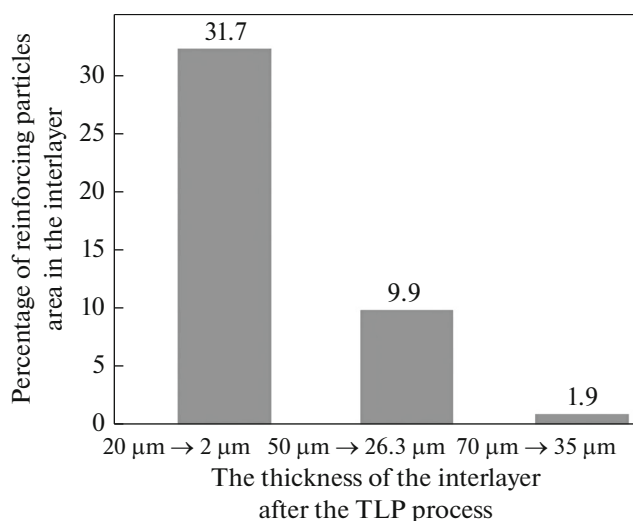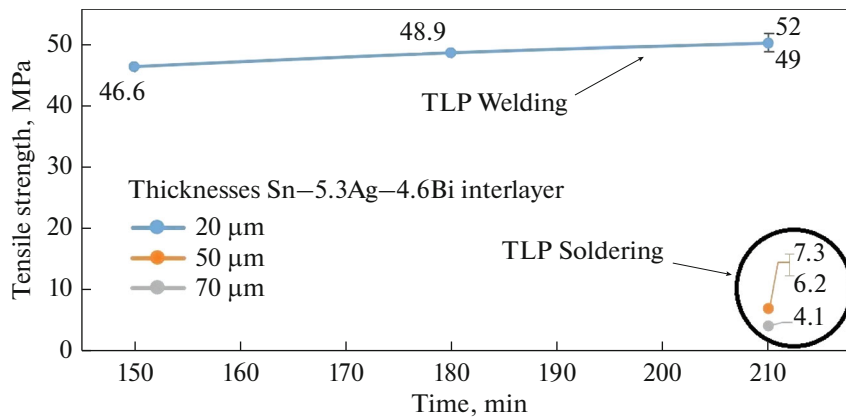
Fig. 6. Tensile strength of the joints vs. thickness for Sn−5.3Ag−4.6Bi interlayer at 453°C.
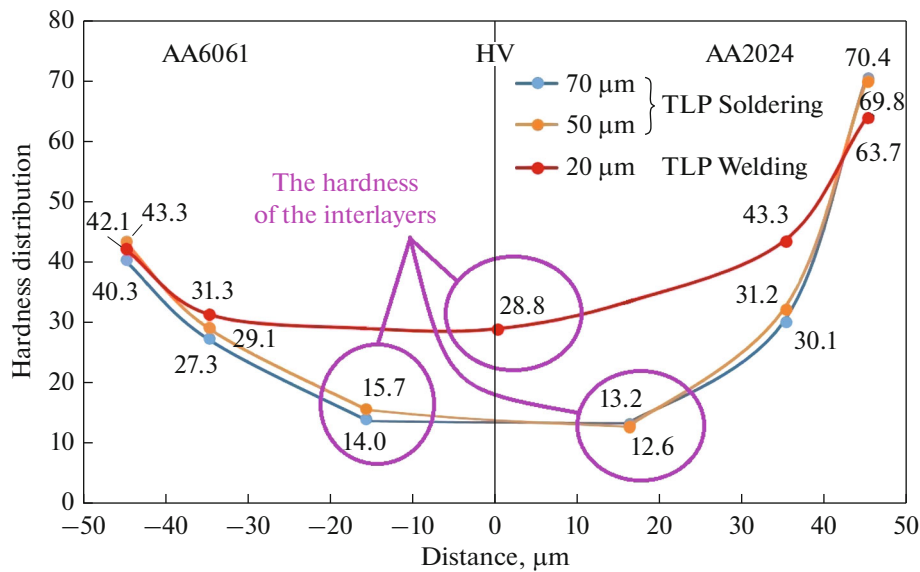

Fig. 7. Microhardness profile of diffusion zone at bonding time of 210 min in Sn−5.3Ag−4.6Bi with thicknesses of 20, 50, and 70 μm.

of tin in the soldering mode ranged from 3 to 10 μm, depending on the position and base alloy material. Moreover, the penetration depth of the experiment is always less than the modeling, as modeling assumed pure aluminum. In this paper, TLP soldering at 453°C is defined as stage 3, and in TLP welding mode is defined as stage 4 of the TLP process in reference [3]. Over time, the structure process becomes more homogeneous.

CONCLUSIONS

(1) Based on the modeling results, Sn (90.1 wt %) can diffuse up to 23 μm at 453°C and bonding time of 210 min. After an hour at the mentioned condition, Sn diffused to a distance of 12 μm. After one day at this temperature, the Sn content reached 2 wt % at the 50 μm distance from the interlayer boundary with the Al base. (2) Based on the modeling results, Ga (90.1 wt %) can diffuse up to 9 μm at 453°C and the bonding time of 210 min. After 15 h and 3 days at the mentioned condition, Ga diffused to a distance of 20 and 44 μm, respectively. (3) Based on the modeling results, Zn (90.1 wt %) can diffuse up to 8 μm at 453°C and the bonding time of 210 min. After 15 h and 3 days at the mentioned condition, it diffused to a distance of 18 and 40 μm, respectively. (4) The maximum tensile strength of the welding for 210 min was 52 MPa for 20 μm thickness Sn−5.3Ag−4.6Bi interlayer. (5) Diffusion of Al, Ag, Cu, Mg, and Sn creates $AlAg_3$, Cu_6Sn_5, Al_2Cu, and $Mg_{45}Al_{40}Ag_{15}$ in the interlayer. ($Mg_{45}Al_{40}Ag_{15}$ is an Ag-rich $γ(Al_{12}Mg_{17})$). (6) Compared to Al, Cu penetrated further into the Sn−5.3Ag−4.6Bi interlayer at 453°C. (7) By prolonging the process, the bond strength increased due to the time-consuming process of atomic diffusion at a con-

stant temperature. (8) In the experiments, the joint hardness was always lower than the base metals. (9) By increasing the Sn−5.3Ag−4.6Bi interlayer thickness (20−70 µm), the average tensile stress decreased. (10) By decrementing the interlayer thickness, the size of the reinforcing particles significantly decreased while their number showed a rise. (11) Based on the modeling results, for Sn−5.3Ag−4.6Bi interlayer thicknesses below 23 µm, the mixing will be augmented in such a way that welding occurs at 453°C for 210 min. Higher thicknesses will lead to soft soldering under the same conditions.

FUNDING

CONFLICT OF INTEREST

The authors declare that they have no conflicts of interest.

REFERENCES

1. "Aerospace Specification Metals Inc (ASM)," ASM Material Data Sheet- 800 398-4345, Aluminum 2024-O. (1987).

2. "Standard Specification for Aluminum and Aluminum-Alloy Sheet and Plate (Metric)," ASTM- Designation: B209M-14. (2014).

3. W. D. MacDonald, T. W. Eager, "Transient Liquid Phase Bonding," Ann Rev. Mater Sci. **22**, 23−46 (1992).

4. D. L. Olson, D. L. "Welding, Brazing, and Soldering," ASM Handbook, Vol. 6, 343 (1993).

5. M. Xiong, L. Zhang, L. Sun, P. He, W. Long, "Effect of CuZnAl particles addition on microstructure of Cu/Sn58Bi/Cu TLP bonding solder joints," Vacuum. **167**, 301−306 (2019).

6. J. X. Zhang, R. S. Chandel, Y. Z. Chen, H.P. Seow, "Effect of residual stress on the strength of an alumina− steel joint by partial transient liquid phase (PTLP) brazing," Journal of Materials Processing Technology. **122**, Issues 2−3, 220−225 (2002).

7. H. Baker, "Alloy Phase Diagrams," ASM Handbook. Vol. 3, Chap. 2, pp. 44 and 48 (1993).

8. E. F. Bradley, Superalloys and their application, "in SuperalloysöA Technical Guide, ASM International," Metals Park, Ohio, 22−28 (1988).

9. "Aerospace Specification Metals Inc (ASM)," ASM Material Data Sheet- 800-398-4345, Aluminum 6061-O. (1987).

10. J. T. Chien, Y. Jiao, "Numerical simulation of solute redistribution during transient liquid phase bonding process for Al−Cu alloy", Numer. Heat Transfer, Part A. **39**, 123−138 (2001).

11. A. N. Alhazaa, T. I. Khan, I. Haq, "Transient liquid phase (TLP) bonding of Al7075 to Ti−6Al−4V alloy," Mater. Charact. **61**, 312−317 (2010).

12. A. N. Alhazaa, T. I. Khan, "Diffusion bonding of Al7075 to Ti−6Al−4V using Cu coatings and Sn−3.6Ag−1Cu interlayers," J. Alloys Compd. **494**, 351−358 (2010).

13. M. S. Kenevisi, S. M. Mousavikhoie, "A study on the effect of bonding time on the properties of Al7075 to Ti−6Al−4V diffusion bonded joint," Mater. Lett. **76**, 144−146 (2012).

14. M. S. Kenevisi, S. M. Mousavikhoie, "An investigation on microstructure and mechanical properties of Al7075 to Ti−6Al−4V transient liquid phase (TLP) bonded joint," Mater. Des. **38**, 19−25 (2012).

15. M. Samavatian, A. Halvaee, A. Amadeh, A. Khodabandeh, "An investigation on microstructure evolution and mechanical properties during liquid state diffusion bonding of Al2024 to Ti−6Al−4V," Mater. Charact. **98**, 113−118 (2014).

16. M. Samavatian, A. Halvaee, A. Amadeh, A. Khodabandeh, "Transient liquid phase bonding of Al 2024 to Ti−6Al−4V alloy using Cu−Zn interlayer," Trans. Nonferrous Met. Soc. China. **25**, 770−775 (2015).

17. A. Anbarzadeh, H. Sabet, M. Abbasi, "Effects of successive-stage transient liquid phase (S-TLP) on microstructure and mechanical properties of Al2024 to Ti−6Al−4V joint," Mater. Lett. **178**, 280−283 (2016).

18. A. Anbarzadeh, H. Sabet, A. R. Geranmayeh, "An Investigation on the Modeling of Heat Distribution and Atomic Diffusion in the Joining of the AA2024-T4 to AA6061-T6 by TLP Process," Journal of Environmental Friendly Materials **4** (2): 21−25 (2020).

19. M. N. Mangomedov, "On the criterion of the crystal-Liquid Phase Transition," Journal of The Physics of Metals and Metallography **105**, No. 2, 116−125 (2008).

20. A. Anbarzadeh, H. Sabet, A. R. Geranmayeh, "Investigation of microstructure and tensile strength of TLP in the joint of AA2024-T4 alloys to AA6061-T6 using Sn-2.4Bi interlayer," 3rd International Conference on Welding and Non-Destructive Testing (ICWNDT 2021) (in Persian).

21. H. Y. Zhao, J. H. Liu, Z. L. Li, Y. X. Zhao, H. W. Niu, X. G. Song, H. J. Dong, "Non-interfacial growth of Cu3Sn in Cu/Sn/Cu joints during ultrasonic-assisted transient liquid phase soldering process," Mater. Lett. **186**, 283−288 (2017).

22. L. Sun, M. H. Chen, L. Zhang, "Microstructure evolution and grain orientation of IMC in Cu-Sn TLP bonding solder joints," J. Alloys Compd. **786**, 677−687 (2019).

23. T. H. Lee, Y. J. Lee, K.T. Park, H. H. Nersisyan, H. G. Jeong, J. H. Lee, "Controlling Al/Cu composite diffusion layer during hydrostatic extrusion by using colloidal Ag," J. Mater. Process. Technol. **213**, 487−494 (2013).

24. O. Fornaro, "Directional Solidification of Sn-Cu6Sn5In Situ Composites," Adv. Mater. Sci. Eng., Article ID 9210713. 1−9 (2019).

25. J. W. Xian, Z. L. Ma, S. A. Belyakov, M. Olivier, C. M. Gourlay, "Nucleation of tin on Cu_6Sn_5 layer in electronic interconnections," Acta Mater. **123**, 404−415 (2017).

26. D. D. Maio, C. P. Hunt, "Time-lapse photography of the β-Sn/α-Sn allotropic transformation," J. Mater. Sci. : Mater. Electron. **20**, 386−391 (2008).

27. W. Peng, "An investigation of Sn pest in pure Sn and Sn-based solders," Microelectron. Reliab. **49**, 86−91 (2009).

28. W. J. Plumbridge, "Tin pest issues in lead-free electronic solders," J. Electron. Mater. **18** (1), 307−318 (2007).

29. B. Cornelius, S. Treivish, Y. Rosenthal, M. Pecht, "The phenomenon of tin pest: A review," Microelectron. Reliab. **79**, 175−192 (2017).

30. N. A. Belov, O. O. Stolyarova, T.I. Muraveva, D. L. Zagorskii, " Phase Composition and Structure of Aluminum Al−Cu−Si−Sn−Pb Alloys", Journal of The Physics of Metals and Metallography, **117**, No. 6, 600−608 (2016).

31. V. V. Bryukhovetskii, V. P. Poyda, R. I. Kuznetsova, K. A. Mohammoud, D. E. Pedun, " Phase Transformations and Structural Changes in the Course of the High-Temperature Superplastic Deformation of Aluminum Alloys" Journal of The Physics of Metals and Metallography **110**, No. 6, 588−596 (2010).

32. G. Erdelyi, K. Freitag, H. Mehrer, "Diffusion of tin implanted in aluminium," Philos. Mag. A. **63**, 1167−1174 (1991).

33. H. Mehrer, "Diffusion in Solids," Springer series in solid-state sciences. pp. 333− Fig. 19.2 (2007).